Reactive Gelation Synthesis of Monodisperse Polymeric Capsules Using Droplet-Based Microfluidics

Tianjin Yang, Alberto Cingolani, Tommaso Casalini, Abdessalem Aribia, Antoine Klaue, Hua Wu, Stavros Stavrakis, Andrew de Mello, and Massimo Morbidelli**

A novel methodology, combining reactive gelation and droplet-based microfluidics, is described for the synthesis of rigid, porous, and hollow polymeric nanoparticles (NPs). The precursors of such capsules are microfluidically generated latex droplets, with diameters tunable between 20 and 100 µm. The conversion of latex droplets to polymeric capsules involves two steps, namely self-migration and gelation of the NPs toward the oil–water interface to form a solid-like shell, and then postpolymerization to covalently fix the shell structure. The hollow structure of the capsules results from the interaction between negatively charged NPs inside the droplet and positive charges present on fluorosurfactant at the droplet interface. Significantly, the porosity and average pore size in the capsule shell can be controlled through variation of the initial NP concentration in the droplet. Based on the analysis of diffusion of fluorescent molecules of known size, it is shown that penetration of molecules into the internal volume of the capsules increases as the initial NP concentration in the droplet decreases, thus the porosity of the formed shell increases. This novel synthetic methodology defines a powerful tool in the generation of hollow capsules of controlled size and morphology, and has significant application in material sciences.

1. Introduction

Porous materials in the form of microscale particles (MPs) or microcapsules of controlled morphology are of significant interest and utility in pharmaceutical and materials sciences,[1] and have found wide use in separation and purification techniques,[2] catalysis,[3] thermal insulation,[4] drug delivery,[5] and tissue engineering.[6] Recent advances in the synthetic processing of porous particles have engendered new ways of fabricating materials of bespoke size, shape, composition, and functionality.[7] Conventional approaches for synthesizing porous particles are commonly based on suspension polymerization in the presence of a porogen.[7] However, a large degree of versatility and control can, in principle, be introduced using colloidal techniques.[8] For example, self-organization of colloidal particles at fluid–fluid interfaces,[9] templating,[10] and controlled aggregation[11] can result in the generation of MPs of controllable morphology, ranging from spheres to rather complex structures. For example, porous MPs in the forms of crystals,[12] capsules,[8a] hollow shells,[13] and nonspherical templated arrangements[14] have been produced and used in a variety of applications. A key species in this new generation of porous MPs is the colloidosome,[8b] a microscale capsule whose shell is composed of colloidal polymer particles. Colloidosomes have found significant application in the fields of microencapsulation and triggered release,[15] and can be prepared through the self-assembly of colloidal particles at an oil/water interface, cf. classical Pickering emulsions.[16] Here, porosity is controlled by the interstitial spaces between individual colloidal particles and by defects in their surface arrangement. To make such MPs usable in practical applications, structures must be "hardened" to some degree to provide mechanical resistance.[15] Thermal annealing,[17] covalent crosslinking,[18] and additional polymerization at the interface[19] all represent promising options, but the former approach requires the use of high temperatures (above the T_g). In addition, crosslinking and polymerization are often compromised by the scarcity of chemicals that are compatible in both phases and the need for complex multiscale protocols.[15]

To address the above deficiencies, Marti et al. introduced reactive gelation as a robust method to make mechanically stable porous polymer networks.[20] The basic technique involves multiple steps. First, an aqueous dispersion of colloidal polymer nanoparticles (NPs; e.g., latex) is swollen by a mixture of monomer and initiator. Second, controlled aggregation or templating is used to "arrange" particles into a defined structure. This is followed by a postpolymerization (via heating at temperatures between 50 and 70 °C) to harden and consolidate the previously formed network, thus ensuring mechanical stability.

Recently, droplet-based microfluidics has emerged as a promising and potentially powerful platform for the synthesis and assembly of porous MPs. Critically, the adoption of

Dr. T. Yang, Dr. A. Cingolani, Dr. T. Casalini, A. Aribia, Dr. A. Klaue, Dr. H. Wu, Dr. S. Stavrakis, Prof. A. de Mello, Prof. M. Morbidelli
Institute for Chemical and Bioengineering
Department of Chemistry and Applied Biosciences
ETH Zurich
Vladimir-Prelog-Weg 1, 8093 Zürich, Switzerland
E-mail: andrew.demello@chem.ethz.ch; massimo.morbidelli@chem.ethz.ch

The ORCID identification number(s) for the author(s) of this article can be found under https://doi.org/10.1002/admt.201900092.

DOI: 10.1002/admt.201900092

segmented flows allows the precise tuning of not only process parameters, but ultimately the morphology of the synthesized MPs.[21] As previously noted, the simplest route to introducing porosity in MPs is through the addition of a porogen. To this end, Dubinsky et al. presented a method based on copolymerization of ethylene glycol dimethacrylate and glycidyl methacrylate within droplets to produce porous MPs.[22] Various solvents (such as diethyl phthalate, diisobutyl phthalate, dioctyl phthalate, and diisodecyl phthalate) that are inert to the monomer and initiator were used as porogens. In contrast to induced phase separation occurring within the monomer/porogen droplets, application of high internal phase emulsions (a special type of emulsion where the volume fraction of the dispersed phase can be up to 0.99) provided for excellent control over both bead porosity and shape.[23] Using the same concept (i.e., avoiding use of a porogen), Watanabe et al. reported the formation of porous polymeric MPs via solvent extraction and microfluidic emulsification.[24] This approach allowed the generation of "smooth skinned" MPs containing gradients in internal pore structure. Finally, solvent evaporation/diffusion from droplets consisting of stabilized particles dispersed in a solvent can be used to produce porous silica structures,[25] biodegradable microspheres,[26] and polymeric microcapsules.[27]

Herein, we propose a novel and general methodology that combines reactive gelation and microfluidics to produce monodisperse, rigid, hollow, and spherical microparticles with tunable shell porosity. The approach relies on and leverages a newly observed gelation phenomenon, involving interfacial self-aggregation of primary NPs. Furthermore, we propose a possible mechanism by which the assembly of the aforementioned hollow MPs occurs and verify this using molecular dynamics (MD) simulations. A primary result of this work is the design of hollow, porous capsules of controllable porosity and shell thickness.

2. Results and Discussion

2.1. Microfluidic Preparation of Porous Hollow Microparticles

Initial experiments used the picoinjector microfluidic platform (Figure S1a, Supporting Information) to screen gelation conditions through variation of salt and latex concentrations. In brief, latex droplets formed at the flow focusing geometry traveled downstream until they arrived at the picoinjector unit, where an electric field was applied. This causes breakage of the droplet surfactant membrane and injection of a controlled volume of salt solution. Picoinjection is a well-established technique droplet-based microfluidic experiment since it allows for the injection of defined (picoliter) volumes of reagent into individual droplets.[28] After the formation of a gel framework within the droplets, postpolymerization was initiated at 50 °C, resulting in the consolidation of the framework and the formation of solid, monodisperse capsules. It is important to note that throughout the entire process, droplets remain stable and do not coalesce. This is primarily due to the presence of the triblock fluorosurfactant in the oil phase, which migrates to the oil–water interface and stabilizes the droplets. Subsequent to postpolymerization, porous capsules were rinsed and dried under vacuum to a powder.

As shown in **Figure 1**a,b, the picoinjector is successful in allowing the precise injection of a controllable amount of salt (e.g., sodium chloride) solution into latex droplets. The injected salt solution destabilizes the primary NPs within droplets, leading to their aggregation as ionic strength increases and their repulsive interaction barrier decreases. As observed in Figure 1a, at high salt concentrations (0.75 M), aggregation within droplets is extremely rapid and occurs along the visible portion of the channel. Conversely, Figure 1b indicates that at low salt concentrations (0.125 M), aggregation does not occur on the same timescale. In principle, however, it is always possible

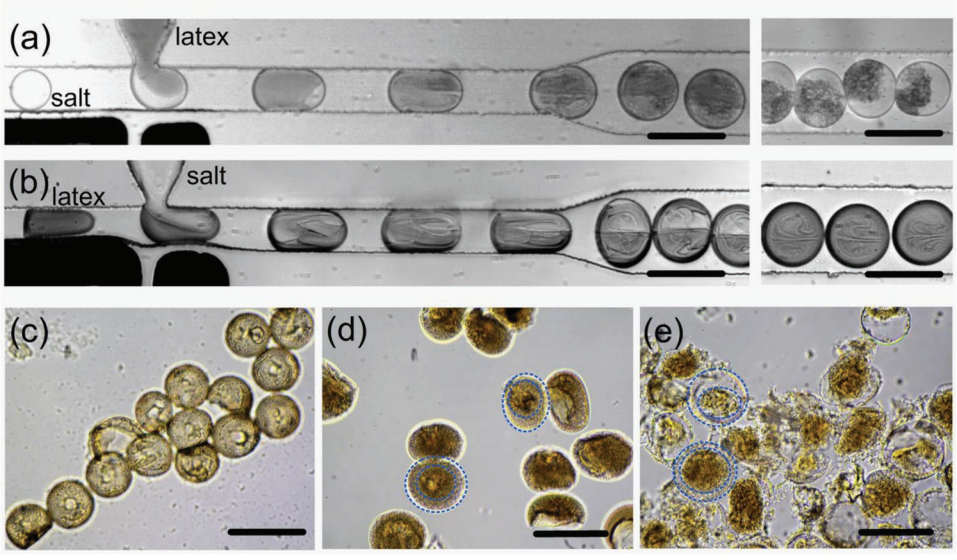

Figure 1. a) Latex is injected into a 1 M sodium chloride aqueous solution droplet at a volume ratio of 0.7, with fast aggregation of the primary NPs occuring on chip. b) A 0.3 M sodium chloride aqueous solution is injected into a latex droplet at a volume ratio of 0.5. Slow aggregation of primary NPs is observed on chip. c) Formation of a solid-like shell without salt addition. d) An intermediate state observed at extremely low salt concentrations, where, apart from the solid-like shell, a piece of gel is also formed inside the hollow sphere. e) Latex droplets injected with a high salt concentration, leading to fast aggregation. Scale bars: 100 µm.

to control both the salt and NP concentrations such that NP aggregation leads to the formation of growing clusters that eventually percolate and lead to a jammed, kinetically arrested state.[11,29] Such a liquid-to-solid transition is typically referred to as gelation, where the shape of the formed gel is defined by the shape of the container in which gelation occurs. In the case of the latex droplets generated in our microfluidic system, experiments at various salt and NP concentrations showed that it was difficult to controllably tune aggregation conditions to convert the spherical latex droplets to spherical gels. Instead, and as shown in Figure 1d (salt concentration 0.125 M), only small gel sections were formed inside each droplet. This is most likely due to the fact that the wall of the container (the droplet) is not rigid, but soft and deformable. This means that the wall itself can be altered by gelation, an intrinsically inhomogeneous process. Second, the percolation of clusters to form a gel occurs only when the occupied volume of clusters becomes comparable to the volume of the droplet. In other words, clusters will only percolate to form a gel when the space of the container limits further growth. In the present case, since the container is a soft droplet, its shape may change or even be broken, with the total occupied volume of the clusters even being larger than the volume of the droplet. Considering both aspects, the conversion of a spherical droplet into a spherical gel becomes a rare event. Accordingly, in the presence of a salt concentration close to 0.75 M (Figure 1e), a mixture of deformed gels, gel fragments, and even broken shells after gelation were obtained. Conversely, it is interesting to note that, if no salt was added, primary NPs in a droplet were able to migrate toward the interface and eventually aggregate to form a hollow sphere of the same shape as the droplet, and with a porous shell, as indicated in Figure 1c.

A possible explanation of these findings is that the migration of NPs toward the droplet–carrier phase interface is controlled by electrostatic interactions between sodium dodecyl sulfate (SDS) inside the droplet and the triblock fluorosurfactant in the oil phase.[30] In particular, at the aqueous–oil interface, the hydrophilic polyethylene glycol (PEG) portion of the triblock fluorosurfactant will be directed toward the water phase, and at pH values between 3 and 4 in the droplet, the PEG block may possess some degree of positive charge.[31] Consequently, since primary NPs are negatively charged by SDS, as well as $S_2O_8^{2-}$ from the initiator,[32] they will move toward the interface due to electrostatic attraction. Such a phenomenon has already been described for similar systems.[31,33] In addition, since adsorbed SDS molecules on the NP surface can desorb and associate with the interface, NP stability can be reduced, leading to NP aggregation near the interface, and the formation of the solid-like shell. This process can be further facilitated by crowding of the NPs at the interface. A proposed scheme describing this mechanism is presented in **Figure 2**. In this respect, we have

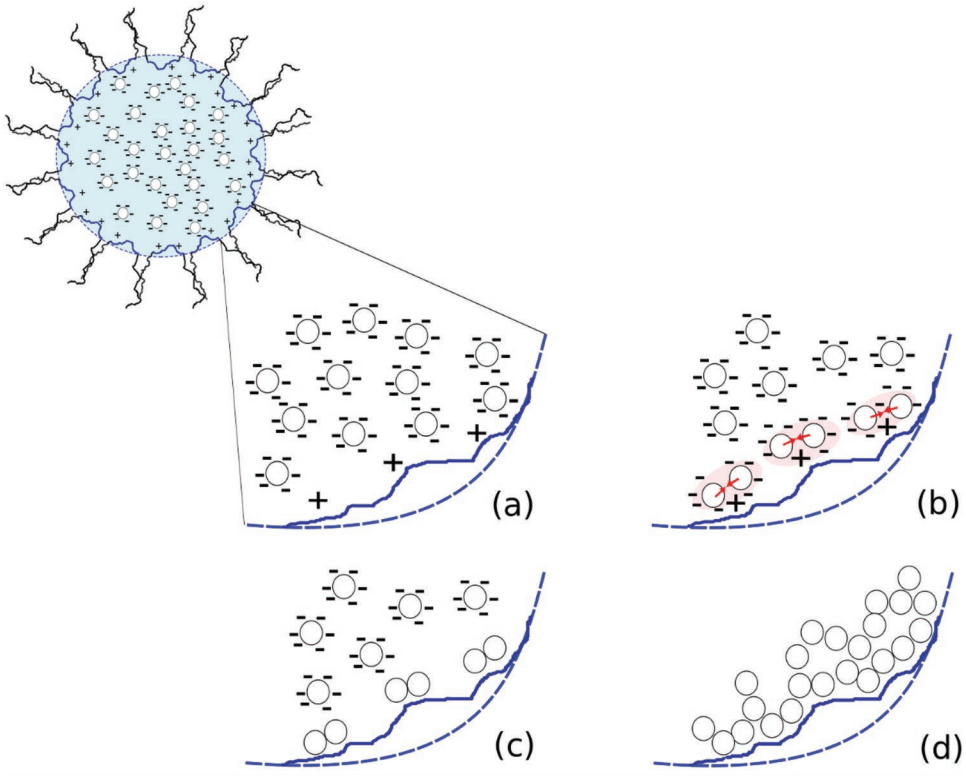

Figure 2. Schematic representation of the mechanism of formation of hollow porous capsules. a) The negatively charged NPs in the droplet are attracted by positive charges present on hydrophilic part of the fluorosurfactant used to stabilize the droplet itself. b) The positive charges partially screen the negative ones, which stabilize the NPs in the latex, and allow them to get close enough to aggregate. Moreover, some SDS molecules can partially dissociate from the NPs, reducing their stability even more. c) Aggregation continues all over the internal surface of the droplet until a percolating structure forms. d) With the shape of the original droplet, a solid-like shell is formed, which is hardened and preserved after postpolymerization, allowing the production of a porous, hollow, and mechanically stable capsule.

also observed that at very low salt concentrations, apart from the formation of a solid-like shell, gel pieces can also form inside the hollow sphere (see the dashed circle in Figure 1d), resulting from the competition between salt-induced gelation and interface-induced migration to the interface.

It is worthy of mention that electrostatic attraction is certainly not the only driving force for NP migration. For example, it is well known that NPs may self-organize at the interface between two immiscible fluids, due to a reduction in the free energy of the system, and such forces have been widely exploited to produce templated materials.[9a] On the other hand, this cannot be the prevailing mechanism in the current situation, since we observe that NPs alone are unable to stabilize the latex droplets in oil in the absence of the triblock fluorosurfactant. Moreover, the presence of the surfactant should prevent possible interfacial jamming due to water migration within the oil domain. This description is also supported by the observed correspondence between the size of the generated droplets and that of the final dry particles. From the above discussion, it is clear that when using droplet-based microfluidics to produce microscale capsules of well-controlled structure, one should avoid using salts to destabilize NPs within droplets. Instead, the presence of other forces at the oil–water interface (i.e., electrostatic attraction in the current case) might motivates NPs toward interface, leading to hollow MPs formations. In this sense, the observed process of gelation at the oil–water interface is a newly described phenomenon, which has yet to be described or exploited in the current literature.[34]

The obtained capsules are hollow porous spheres of the same size as the initial latex droplets. Postpolymerization fixes the shell structure to form a hard, mechanically stable capsule. The mechanical robustness of the microcapsules was verified via scanning electron microscopy (SEM) analysis after several washing steps. It should be noted that such robustness is not especially surprising, since, reactive gelation allows the production of polymer structures able to withstand loads in chromatography and volumetric flows up to 9 mL min^{-1}.[8e,20,32] Use of the flow focusing platform allows different sized capsules (having diameters between 20 and 80 μm and a high degree of monodispersity) to be generated through alteration of the volumetric flow rates of the input streams and the channel diameter (**Figure 3**). The size distribution of the latex droplets resulting from our system was determined via image analysis,[35] with a representative size histograms being shown in Figure 3. As can be seen, each droplet population (between 800 and 900 droplets) exhibits a low degree of polydispersity, with average diameters of 17.08 ± 0.13 μm, 34.88 ± 0.79 μm, 59.86 ± 1.12 μm, and 80.28 ± 2.02 μm, respectively. Additionally, the sizes of the spherical and hollow capsules match well with the sizes obtained from the corresponding SEM images (Figure 3, insets). As discussed, the size distribution of the final hollow capsules, based on the formation mechanism, is directly controlled by the size distribution of the initial droplet population. Inspection of the SEM images taken at higher magnifications, and as shown in **Figure 4**a,b, reveals that the packing of NPs within the shell of the hollow capsules is rather disordered. This feature confirms that the solid-like shell results from

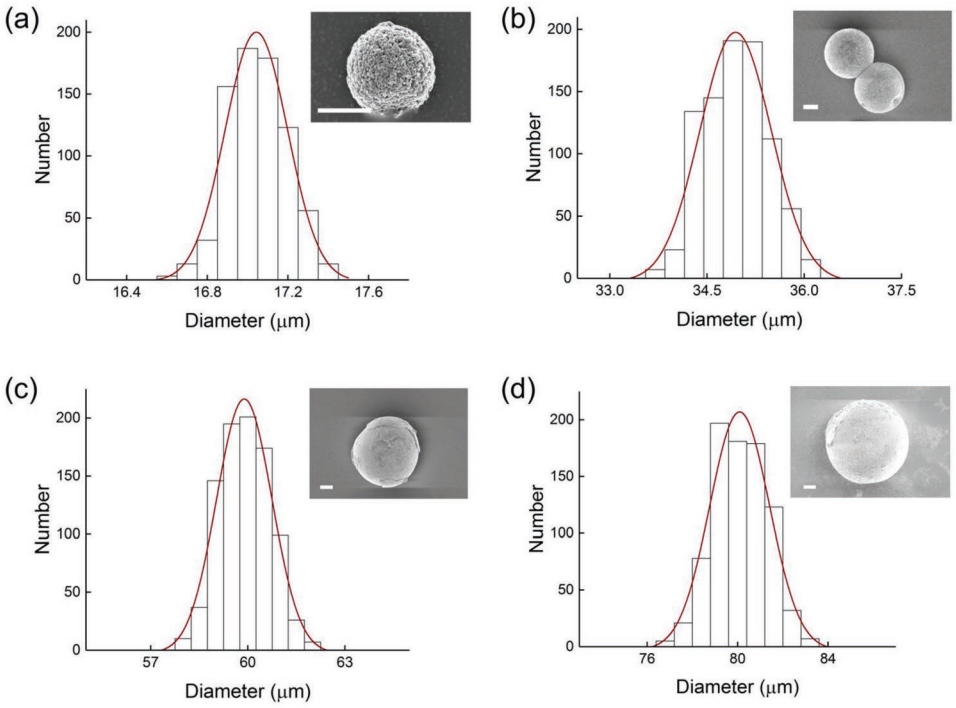

Figure 3. Size distributions for four populations of latex droplets and the SEM images of porous hollow capsules obtained in each population. The diameters of the droplets are a) 17.08 ± 0.13 μm, generated under a latex/oil flow rate of 8/15 μL min^{-1}, b) 34.88 ± 0.79 μm, generated under a latex/oil flow rate of 10/11 μL min^{-1}, c) 59.86 ± 1.12 μm, generated under a latex/oil flow rate of 6/4 μL min^{-1}, and d) 80.28 ± 2.02 μm, generated under a latex/oil flow rate of 5/2 μL min^{-1}. Scale bars: 10 μm.

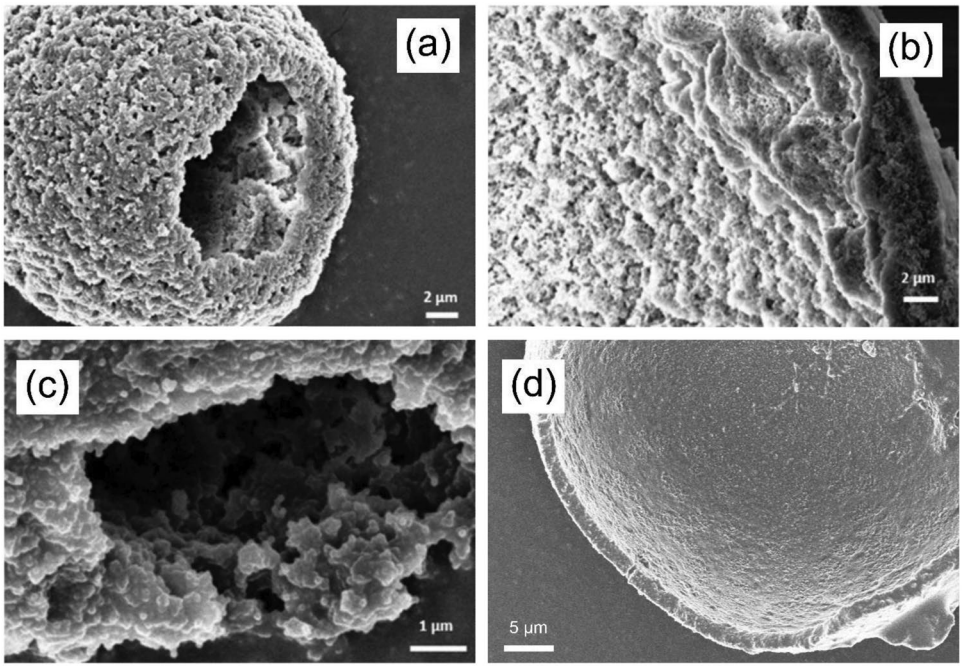

Figure 4. SEM images showing a,b,d) the hollow capsule morphology and the b,c) disordered arrangment of NPs within the capsule shell. The NP concentration is 6 wt% in panels (a) and (c), 8 wt% in panel (b), and 12 wt% in panel (d).

aggregation of NPs. Moreover, NPs partially merge amongst themselves (Figure 4c,d), and in some cases lose their individual identity. This is due to the presence of the monomer-swollen soft shell on primary NPs, which allows partial interpenetration during aggregation.

2.2. Computational Verification of Attraction at the Oil–Water Interface

As discussed, and according to literature data,[31] the oxygen atoms of the PEG block of the fluorosurfactant can present positive charges at pH values between 3 and 4. This will induce an electrostatic attraction between the PEG blocks at the oil–water interface and the polystyrene NPs dispersed in the droplet (since the surface of the polystyrene NPs is negatively charged due to adsorbed SDS). To confirm this view, we performed molecular dynamics simulations, which are described in detail in Section S2 and Table S2 in the Supporting Information. The NP was modeled as a flat surface of amorphous syndiotactic polystyrene (**Figure 5**a), since the chain length of the PEG block is much smaller than the NP diameter. It was assumed that the PEG chain consists of 16 repeating units, and corresponds to a molecular weight of 700 g mol^{-1}. In addition to the SDS used during NP preparation, SDS was added again during the droplet formation process, and our estimation indicates that full coverage of the NP surface by SDS can be assumed correct (Figure 5b). The surface density of SDS is estimated to be 1.7 mg m^{-2}, which is also consistent with prior experimental and computational studies reported in the literature.[36] It is important to note that two specific conditions have been considered for the simulations. First, all the oxygen atoms on the PEG chain are protonated, and second the PEG chain is uncharged. The former is representative of a low pH environment, while the latter is representative of very basic one. These two cases are clearly extremes, and an intermediate situation is expected in real world situations.

In all simulations, the SDS-covered surface was placed in the x–y plane, so as to reproduce an infinite surface by means of periodic boundary conditions. One PEG chain was placed close to the SDS layer, and the surface solvated with explicit water molecules along the z-direction. Explicit sodium ions were added in order to assure electroneutrality. Two different initial conditions were considered for each system (in terms of initial arrangement of the PEG chain on the surface). 100 ns MD simulations were carried out for each model, in an NPT (constant-temperature, constant-pressure) ensemble at 300 K and 1 atm.

Notably, in the case of uncharged PEG, no binding between the PEG chain and the surface is observed during the simulation (Figure 5c), while in the case of fully protonated (charged) PEG, the PEG chain is tightly bound to the adsorbed SDS (Figure 5d). For the latter, the interaction energy was estimated by means of the molecular mechanics Poisson–Boltzmann surface area (MMPBSA) method, which accounts for the relevant contribution of electrostatic interactions in binding. The obtained value of the interaction energy was estimated to be -181.71 ± 21.24 kcal mol^{-1}, where the contribution of van der Waals interactions is limited to -3.39 ± 0.27 kcal mol^{-1}. These results support the presence of electrostatic attractions between the NPs in the droplet and the hydrophilic PEG blocks at the oil–water interface.

2.3. Features of the Formed Capsules

As noted, Figure 4 indicates that packing of the NPs within the shell of hollow capsules is rather disordered, suggesting that the

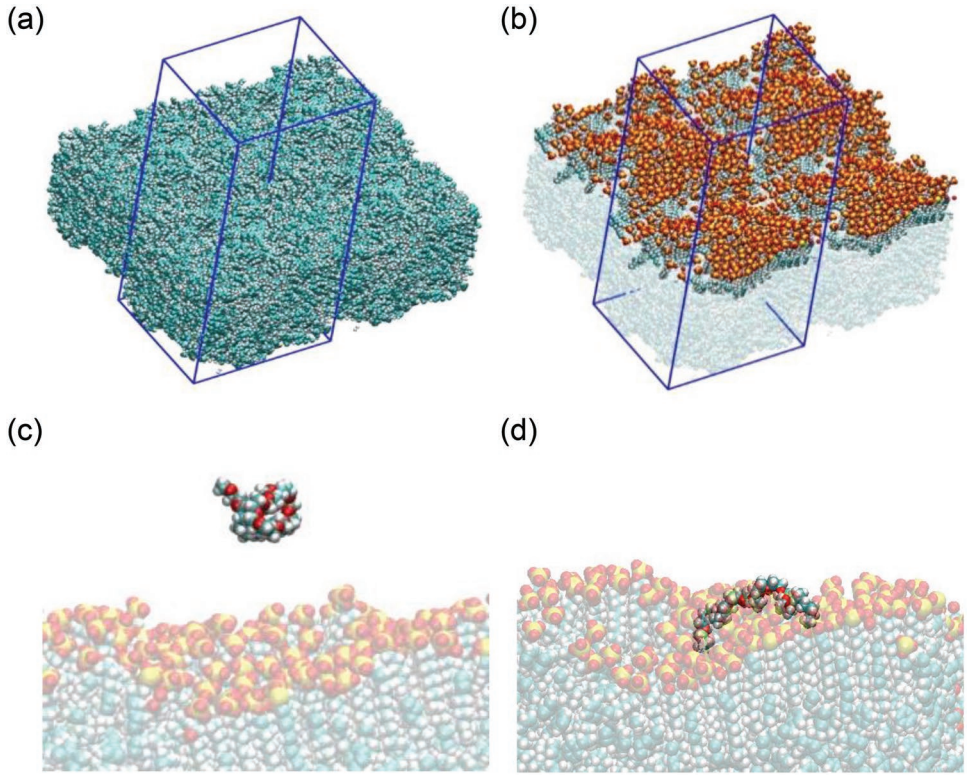

Figure 5. a) The surface of polystyrene (as van der Waals spheres); water and ions are omitted for clarity, replicated along *x*- and *y*-directions, with the simulation box highlighted in blue. b) The polystyrene surface covered with SDS (as van der Waals spheres). c) Interaction with an uncharged PEG chain (no binding occurs). d) Interaction with a protonated PEG chain (surface binding occurs).

solid-like shell results from aggregation/gelation among NPs. Furthermore, no major differences in shell thickness, using different initial latex concentrations, are observed in the SEM images. It is well known that the average size of the clusters constituting a gel strongly depends on the NP concentration,[37] and affects gel morphology.[38] Accordingly, we generated capsules at three NP concentrations, 6.0, 8.0, and 12.0 wt%, respectively, with their SEM pictures being shown in **Figure 6**. In the case of 6.0 wt% particles, it is evident that the solid shell results from interconnection (percolation) of clusters, since the clusters retain their identity. In this case, the pores in the shell are relatively large. Since the size of the clusters forming the gel decreases as NP concentration increases,[37,38] the cluster identity becomes less evident in both the 8.0 and 12.0 wt% cases. Indeed, Figure 6c,f,i shows rather smooth surfaces and small pores for the 12.0 wt% concentration. These results strongly suggest that migration of NPs toward the interface and their subsequent aggregation occur simultaneously, since if aggregation occurs only after NP migration, the morphology of the shell at different NP concentrations would be similar. Finally, based on the characteristics of the gelation process, it is reasonable to expect interconnected pores within the formed capsule's framework.[11]

Porosity and pore size were further verified by assessing shell permeability by confocal fluorescence microscopy. **Figure 7** shows images of capsules prepared at NP concentrations of 6.0, 8.0, and 12.0 wt%, after infiltration with an ethanolic solution of Rhodamine B (0.5×10^{-3} M). It can be seen that Rhodamine B penetration into the capsules increases, NP concentration decreases, confirming that shell porosity and pore size increase. This enables dye molecules to enter the particles and transit the shell. In fact, in Figure 7c, at the highest NP concentration, the dye is located only on the outer surface, because of the compact nature of the shell (Figure 6i).

Finally, we quantified the reduction in concentration of the labeled polymer (fluorescein isothiocyanate-dextran (FITC-dextran 4000)) after diffusion into the internal volume of capsules over a period of 24 h. Representative results are shown in **Figure 8**, where data are reported in the form $(C_0 - C)/(C_0 \times m_p)$, where C_0 represents the initial FITC-dextran 4000 concentration, C the concentration after 24 h, and m_p is the dried mass of porous capsules. It is observed that the decrease in the dye concentration reduces as a function of NP concentration. This result further confirms that porosity and pore size in the shell decrease as the NP concentration increases. Accordingly, we can conclude that the initial NP concentration in the droplets is an important parameter affecting the arrangement of NPs within the capsule shell, and thus the porosity, pore size, and size distribution of hollow capsules.

3. Conclusions

The studies described herein have successfully combined reactive gelation and microfluidics to synthesize rigid and hollow polymeric capsules, with an average diameter that

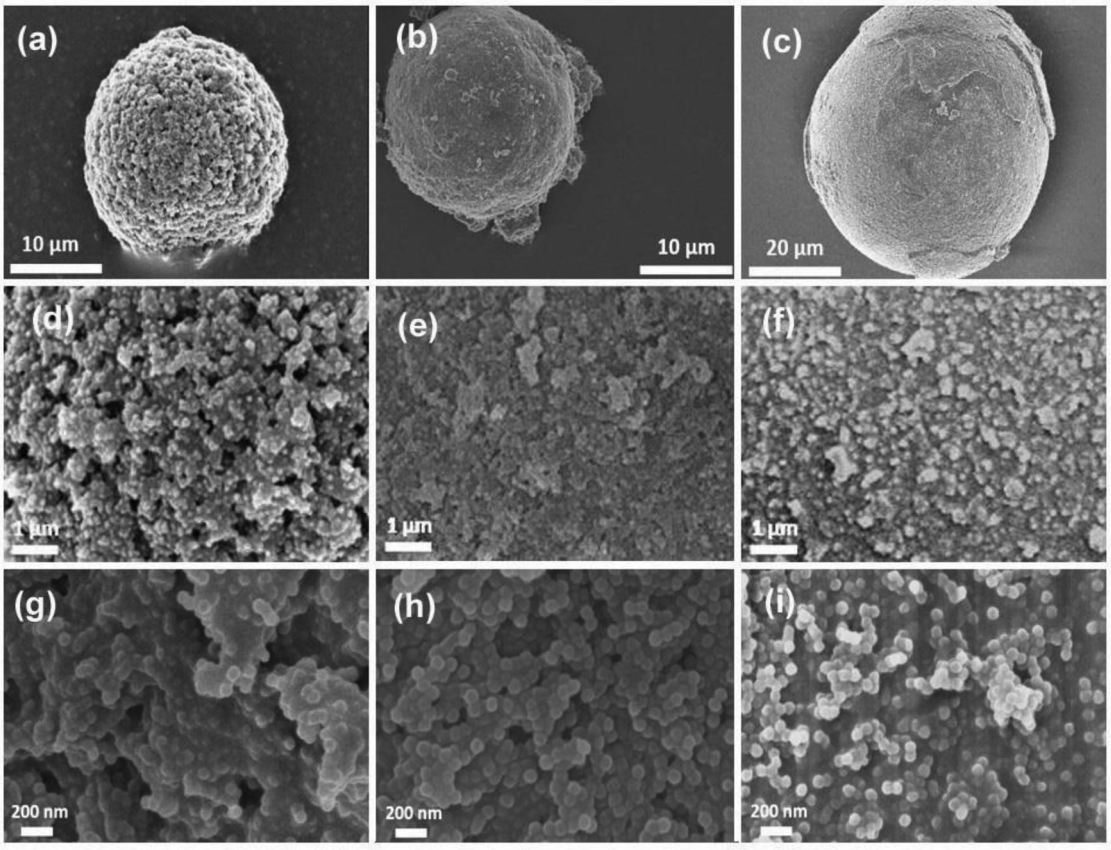

Figure 6. SEM images of capsules and their corresponding surfaces, produced at the initial NP concentrations of a,d,g) 6 wt%, b,e,h) 8 wt%, and c,f,i) 12 wt%.

can be tuned from 20 to 80 µm, through a newly observed percolation mechanism. Capsule size could be controlled through variation of the size of the precursor droplets. Conversion of latex droplets to porous hollow capsules results from a typical process through which polymer NPs' self-immigrate, while concurrently aggregating, toward the oil–water interface, leading to the formation of a solid-like shell. This might be due to the fact that electrostatic attractions between the negatively charged NPs inside the droplet and the positively charged PEG block of the fluorosurfactant at the interface play a key role in the mechanism; a fact supported by both experimental studies and molecular dynamic simulations. The porosity and pore size in the shell of the capsule are shown to decrease with NP concentration, without a major effect on shell thickness, as shown in Figure 4. This confirms that the solid-like shell is formed through aggregation, a kinetically arrested process (gelation) rather than a thermodynamically driven one (self-assembly), through post-polymerization. The shell structure can be consolidated, and rigid, hollow, and permeable capsules are produced and collected. As expected, different surface porosity results in variable permeability and accessibility to molecular species. Accordingly, we have shown both qualitatively and quantitatively that penetration into the internal volume increases as the initial NP concentration in the droplet decreases, thus indicating that porosity and the pore size in the formed shell increase.

The combination of reactive gelation and microfluidics, taking advantage of a newly observed gelation phenomenon,

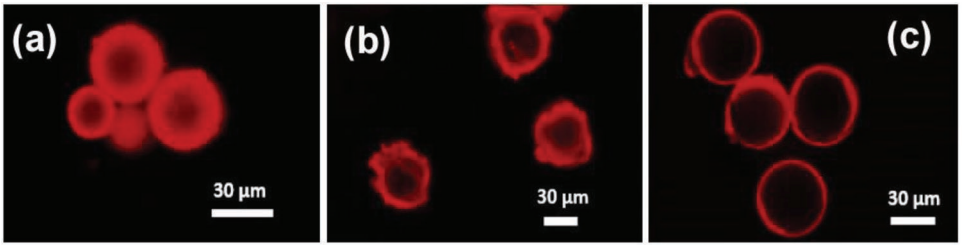

Figure 7. Confocal fluorescence images of capsules produced using an initial NP concentration of a) 6 wt%, b) 8 wt%, and c) 12 wt%, and after immersion in a Rhodamine B solution for 24 h.

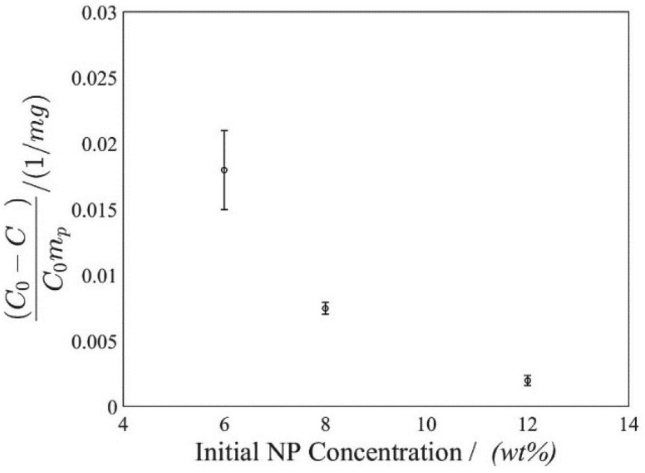

Figure 8. The measured concentration reduction (per unit mass of added capsules) of FITC-dextran 4000 in solution 24 h after capsules addition as a function of the initial NP concentration used in capsule production.

results in a robust and efficient method for producing rigid, porous, and hollow capsules. The developed process provides a unique tool to control capsule morphology and permeability since both play crucial roles in applications such as the trap and release of species in the pharmaceutical and materials sciences. This offers an innovative path, not only to miniaturizing microchannel emulsification reactors and preparing monodisperse spherical capsules, but also in achieving unprecedented control over the structure and shape of capsules.

4. Experimental Section

Materials: The following chemicals were purchased from Sigma Aldrich (Buchs, Switzerland) and used without further treatment: styrene (STY, purity ≥ 99 wt%), divinylbenzene (DVB, Technical Grade, >80 wt%), SDS (BioUltra ≥ 99 wt%), sodium phosphate dibasic, sodium phosphate monobasic, and FITC-dextran 4000) with an average molecular weight of 4000. Sodium chloride and potassium persulfate (KPS) were purchased from Merck (Kenilworth, USA). 2-2′-azo (2-methylpropinitirile) (AIBN, purity ≥ 98 wt%) was purchased from Fluka (Morris Plains, USA). These chemicals were used for primary NP production via a semibatch emulsion polymerization conducted through a two-step procedure involving core and shell synthesis as stated previously.[32] Specifically, the NPs used in this work present a highly crossliked (20%) core of 80 nm on which a much softer shell (1%) was grown to reach a total final size of 110 nm. The architecture of the particles was designed as such in order to have partial interpretation of them upon aggregation and ensure mechanical stability.[32]

Rhodamine B was purchased from Acros Organics (Geel, Belgium). Ultrapure grade water was prepared using a Millipore Synergy water purification system (Millipore, Darmstadt, Germany). Water used in all polymerization reactions was de-oxygenated by degassing under vacuum and saturating with nitrogen. 0.5 wt% block copolymer fluorosurfactant was purchased from Ran Biotechnologies (Beverly, USA) and mixed with Novec HFE-7500 fluorinated oil (3 M, St. Paul, USA). Isopropanol was purchased from Fisher Chemicals (Hampton, USA) and used without further treatment.

Microfluidic Device Fabrication: Figure S1 (Supporting Information) presents the microfluidic channel patterns used in the current work. Specifically, microfluidic circuits were designed using AutoCAD 2014 (Autodesk, San Rafael, USA) and printed onto high-resolution film photomasks (Micro Lithography Services Ltd, Chelmsford, UK). Master structures were subsequently fabricated on SU-8 (Microchem Corporation, Westborough, USA)-coated silicon wafers via conventional photolithographic methods.[39] Microfluidic devices were manufactured using standard soft-lithographic techniques. Briefly, a 10:1 wt/wt mixture of polydimethylsiloxane (PDMS) base and curing agent (Sylgard 184; Dow Corning, Midland, USA) was poured over the master structure and cured in the oven at 70 °C for 4 h. The cured PDMS structure was then peeled off the wafer, with inlet and outlet ports being formed using a hole puncher (Technical Innovations, West Palm Beach, USA). The structured PDMS substrate was then bonded to a 3 mm thick, flat PDMS layer using an oxygen plasma (EMITECH K1000X, Quorum Technologies, East Sussex, UK).

In the latex droplet generation device (**Figure 9**b; Figure S1b, Supporting Information), all microchannels were 30 µm high, with the width of the channel after the flow focusing region being 40 µm. Picoinjection devices (Figure 9a; Figure S1a, Supporting Information) were fabricated following the same procedure as previously described. In this approach, droplets pass a channel containing pressurized reagent to be added. Due to the presence of a surfactant layer, the fluid does not immediately enter the droplet, with entry or "picoinjection" being triggered by electrically induced destabilization of the surfactant layer. After substrate bonding, electrodes were formed using solder wire (Stannol, Velbert, Germany). Specifically, the entire microdevice was heated to 180 °C, and low-melting-point solder was injected into the appropriate electrode channel. Cooling the device to room temperature causes the solder to solidify and produce a metallic electrodes.

Latex Droplet Production: A MotionPro Y5 Compact Digital Camera (IDT, Hitchin, UK) and Nikon Eclipse Ti-E microscopy (Nikon Instruments Europe, Amstelveen, Netherlands) were used to monitor and image the droplet formation process. Novec 7500 fluorinated oil containing 0.5 wt% triblock fluorosurfactant was used as the carrier phase and latex containing 0.2 wt% SDS as the discrete phase. Low-pressure dosing modules (neMESYS, Cetoni GmbH, Korbussen, Germany) were used to motivate fluids from 1 mL gastight syringes (Hamilton Bonaduz AG, Bonaduz, Switzerland). Tygon tubing (Cole Palmer, Hanwell, UK) was used to connect syringes to the inlets of the microfluidic device. Latex droplets were formed at the flow focusing geometry (Figure S1b, Supporting Information) with the droplet size being controlled by the ratio of the volumetric flow rates for the continuous and discrete phases (Figure 9b). A picoinjector device (shown in Figure 9a) was used to induce coagulation of primary NPs through injection of an aqueous solution of sodium chloride (at varying concentrations) into the latex droplet. Electrodes were energized using 10 kHz, 500 V AC signals generated by an ADS1102CAL+ digital storage oscilloscope (ATTEN Instruments, Shenzhen, China) and amplified by a high-voltage amplifier (TREK Model 2210, Lockport, USA). The sodium chloride solution was pumped into the injection channel at a constant pressure using a Mitos P-Pump (Dolomite, Royston, UK). Droplet dimensions were analyzed using the open access video processing software Droplet Morphometry and Velocimetry (DMV).[35]

Reactive Gelation: Each latex was diluted with deionized water up to the desired dry mass fraction and swollen by an additional mixture made of DVB and oil-soluble initiator, AIBN (5 wt%). This mixture swells almost exclusively the outer layer (shell) of the NPs, because its crosslinking degree is substantially smaller than that of the core. The amount of added DVB was adjusted to be 10 wt% of the polymer mass of the shell. The obtained dispersion of the swollen NPs was then kept under stirring overnight to ensure complete equilibration. After generation of latex droplets, and the arrangement of the nanoparticles within them in a hollow capsule shape, postpolymerization was used to permanently fix and consolidate the structures and obtain microparticles (Figure 9c). Postpolymerization was conducted by heating the latex droplets at 50 °C for a period of 15 h, enclosed within either a plastic capillary or a 5 mL glass vial, depending on the volume

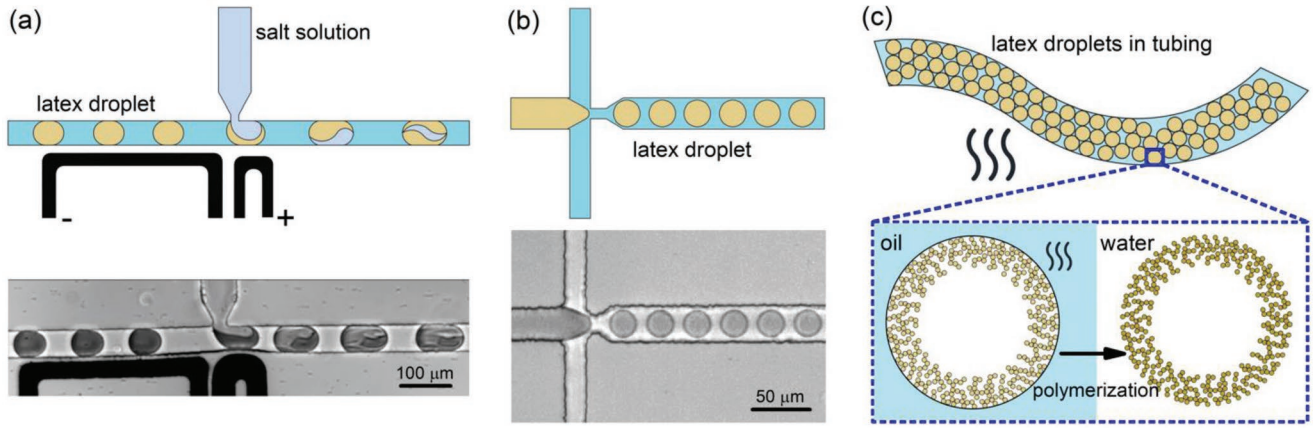

Figure 9. Microfluidic structures and the synthesis workflow used in this study. a) Top: schematic of a picoinjector chip used to screen conditions that lead to particle formation. Bottom: bright field image of salt solution injection into a preformed latex droplet. b) Top: schematic of a flow focusing chip used for the creation of polymer microporous particles. Bottom: bright field image of latex droplets being formed. c) Schematic of the postpolymerization process. After formation of monodisperse aqueous droplets in the oil-stream, polymerization at 50 °C was initiated, resulting in the formation of solid monodisperse particles.

of formed droplets. After postpolymerization, microparticles were washed with an excess amount of isopropanol to completely remove residual oil. Finally, microparticles were fully dried and collected as a powder.

Microparticle Characterization—Morphology: During the entire production process, droplets were constantly monitored via bright-field microscopy. Capsule dispersity after postpolymerization and drying was assessed via SEM using a Gemini 1530 FEG system (Carl Zeiss, Oberkochen, Germany) with a field emission gun operating at 5 kV. For such measurements, samples were coated in platinum.

Microparticle Characterization—Surface Porosity and Permeability of Capsules: The surface porosity and the permeability of capsules were assessed both qualitatively and quantitatively using fluorescent probes. Diffusion of Rhodamine B within the capsule body was monitored using confocal fluorescence microscopy. Specifically, capsules were soaked in isopropanol, in which Rhodamine B was dissolved. After 24 h, the capsules were isolated via centrifugation. Fluorescence images of the capsules were extracted using a Leica SP8-AOBS confocal microscope with an argon laser operating at 514 nm as the excitation beam and a HyD detector for photon collection (Leica Microsystems, Wetzlar, Germany). Bright field images were collected in parallel using a photomultiplier tube (PMT). Quantitative analysis was achieved by measuring the penetration of species of known size (FITC-dextran 4000 has a Stoke's radius of 1.4 nm) within individual porous shells. Exact amounts of dried porous capsules (between 1 and 5 mg) were completely soaked in phosphate buffer at pH 8. Next, when still wet, the whole mass was added to 1 mL of the same buffer, in which a known amount of FITC-dextran 4000 was dissolved. FITC-dextran 4000 concentrations can be directly quantified through measurement of fluorescence intensity. These measurements were performed using a fluorescence plate reader (EnSpire 2300 Multilabel Reader, Perkin Elmer, Waltham, USA).

Once added to the FITC-dextran 4000 solution, the capsules were seen to rapidly sediment. A 200 µL portion of the supernatant was harvested and used to measure the FITC-dextran 4000 concentration; defined forthwith as the initial concentration. Subsequently, capsules were left in the FITC-dextran 4000 solution for 24 h at 4 °C, and the same procedure was repeated to quantify the remaining FITC-dextran 4000 in the supernatant. The relative difference in the two concentrations, divided by the initial mass of the dried capsules, was used to quantify the shell porosity of the capsules. As this point, it should be noted that due to its chemical structure, FITC-dextran 4000 may interact to some degree with the polystyrene surface of the capsule shell and be partially adsorbed. Accordingly, the recorded variation in the concentration may be due to both diffusion into the internal hollow domain and surface adsorption. On the other hand, since all of the capsules were made from the same initial polymer latex, they should present the same interactions with the FITC-dextran 4000.

Simulation for NPs' Molecular Dynamics in Latex Droplet: The behavior of individual NPs inside latex droplets was investigated from a theoretical point of view through a basic molecular scale model and MD simulations. Specifically, a primary NP was modeled as a flat surface made of amorphous syndiotactic polystyrene, while the hydrophilic portion of the surfactant (from the oil phase but located at the oil–water interface) was modeled as pure PEG. The computational protocol could be divided into three phases. In the first, an equilibrated polystyrene surface was built. In the second step, the surface was solvated with explicit water molecules, and explicit SDS molecules being added to realize surfactant adsorption and obtain a reasonable input structure of the stabilized surface. In the last phase, the influence of pH on surfactant/particle interactions was studied. In particular, two different simulations were performed. The first was representative of acidic environments, where PEG oxygen atoms were protonated, and the second mimics neutral/basic pH conditions, where PEG was uncharged. Interaction energies were computed using the MMPBSA method (Section S1, Supporting Information).

Supporting Information

Supporting Information is available from the Wiley Online Library or from the author.

Acknowledgements

T.Y. and A.C. contributed equally to this work. The authors would like to thank Ernesto Scibona for the acquisition of confocal fluorescence images. A.dM acknowledges partial support from a National Research Foundation (NRF) grant funded by the Ministry of Science, ICT and Future Planning of Korea, through the Global Research Laboratory Program (Grant number 2009-00426).

Conflict of Interest

The authors declare no conflict of interest.

Keywords

droplet microfluidics, hollow microparticles, polymer particles, reactive gelation

Received: January 26, 2019
Revised: March 12, 2019
Published online: May 17, 2019

[1] P. Liu, G. F. Chen, *Porous Materials: Processing and Applications*, 1st ed., Butterworth-Heinemann Publication, Oxford **2014**, Ch. 1, pp 1–19.
[2] M. Galia, F. Svec, J. M. J. Frechet, *J. Polym. Sci., Part A: Polym. Chem.* **1994**, *32*, 2169.
[3] P. Kaur, J. T. Hupp, S. T. Nguyen, *ACS Catal.* **2011**, *1*, 819.
[4] L. W. Hrubesh, R. W. Pekala, *J. Mater. Res.* **1994**, *9*, 731.
[5] D. S. Kohane, *Biotechnol. Bioeng.* **2007**, *96*, 203.
[6] H. P. Hentze, M. Antonietti, *Rev. Mol. Biotechnol.* **2002**, *90*, 27.
[7] M. T. Gokmen, F. E. Du Prez, *Prog. Polym. Sci.* **2012**, *37*, 365.
[8] a) T. Bollhorst, K. Rezwan, M. Maas, *Chem. Soc. Rev.* **2017**, *46*, 2091; b) A. D. Dinsmore, M. F. Hsu, M. G. Nikolaides, M. Marquez, A. R. Bausch, D. A. Weitz, *Science* **2002**, *298*, 1006; c) D. F. Schmidt, C. du Fresne von Hohenesche, A. Weiss, V. Schädler, *Chem. Mater.* **2008**, *20*, 2851; d) B. Brand, M. Morbidelli, M. Soos, *Langmuir* **2015**, *31*, 12727; e) A. Lamprou, I. Köse, G. Storti, M. Morbidelli, M. Soos, *Langmuir* **2014**, *30*, 6946.
[9] a) E. Vignati, R. Piazza, T. P. Lockhart, *Langmuir* **2003**, *19*, 6650; b) K. Schwenke, L. Isa, E. Del Gado, *Langmuir* **2014**, *30*, 3069.
[10] a) O. D. Velev, A. M. Lenhoff, *Curr. Opin. Colloid Interface Sci.* **2000**, *5*, 56; b) O. D. Velev, K. Furusawa, K. Nagayama, *Langmuir* **1996**, *12*, 2374.
[11] H. Wu, M. Morbidelli, *Particuology* **2014**, *14*, 1.
[12] G. R. Yi, S. J. Jeon, T. Thorsen, V. N. Manoharan, S. R. Quake, D. J. Pine, S. M. Yang, *Synth. Met.* **2003**, *139*, 803.
[13] E. Loiseau, F. Niedermair, G. Albrecht, M. Frey, A. Hauser, P. A. Rühs, A. R. Studart, *Langmuir* **2017**, *33*, 2402.
[14] a) J. Fan, S. H. Kim, Z. Chen, S. Zhou, E. Amstad, T. Lin, D. A. Weitz, *Small* **2017**, *13*, 1701256; b) J. Y. Sim, J. H. Choi, J. M. Lim, S. Cho, S. H. Kim, S. M. Yang, *Small* **2014**, *10*, 3979.
[15] K. L. Thompson, M. Williams, S. P. Armes, *J. Colloid Interface Sci.* **2015**, *447*, 217.
[16] S. U. Pickering, *J. Chem. Soc., Trans.* **1907**, *91*, 2001.
[17] H. N. Yow, A. F. Routh, *Langmuir* **2009**, *25*, 159.
[18] Y. Chen, C. Wang, J. Chen, X. Liu, Z. Tong, *J. Polym. Sci., Part A: Polym. Chem.* **2009**, *47*, 1354.
[19] Y. Lin, H. Skaff, A. Böker, A. D. Dinsmore, T. Emrick, T. P. Russell, *J. Am. Chem. Soc.* **2003**, *125*, 12690.
[20] N. Marti, F. Quattrini, A. Butté, M. Morbidelli, *Macromol. Mater. Eng.* **2005**, *290*, 221.
[21] B. Wang, P. Prinsen, H. Wang, Z. Bai, H. Wang, R. Luque, J. Xuan, *Chem. Soc. Rev.* **2017**, *46*, 855.
[22] S. Dubinsky, H. Zhang, Z. Nie, I. Gourevich, D. Voicu, M. Deetz, E. Kumacheva, *Macromolecules* **2008**, *41*, 3555.
[23] M. T. Gokmen, W. Van Camp, P. J. Colver, S. A. F. Bon, F. E. Du Prez, *Macromolecules* **2009**, *42*, 9289.
[24] T. Watanabe, C. G. Lopez, J. F. Douglas, T. Ono, J. T. Cabral, *Langmuir* **2014**, *30*, 2470.
[25] N. J. Carroll, S. B. Rathod, E. Derbins, S. Mendez, D. A. Weitz, D. N. Petsev, *Langmuir* **2008**, *24*, 658.
[26] W. J. Duncanson, M. Zieringer, O. Wagner, J. N. Wilking, A. Abbaspourrad, R. Haag, D. A. Weitz, *Soft Matter* **2012**, *8*, 10636.
[27] S. Abraham, Y. H. Park, J. K. Lee, C. S. Ha, I. Kim, *Adv. Mater.* **2008**, *20*, 2177.
[28] A. R. Abate, T. Hung, P. Mary, J. J. Agresti, D. A. Weitz, *Proc. Natl. Acad. Sci. USA* **2010**, *107*, 19163.
[29] M. Y. Lin, H. M. Lindsay, D. A. Weitz, R. C. Ball, R. Klein, P. Meakin, *Nature* **1989**, *339*, 360.
[30] K. C. Tam, E. Wyn-Jones, *Chem. Soc. Rev.* **2006**, *35*, 693.
[31] W. Guo, Y. W. Sun, G. S. Luo, Y. J. Wang, *Colloids Surf., A* **2005**, *252*, 71.
[32] A. Cingolani, D. Baur, S. Caimi, G. Storti, M. Morbidelli, *J. Chromatogr. A* **2018**, *1538*, 25.
[33] L. Bernazzani, S. Borsacchi, D. Catalano, P. Gianni, V. Mollica, M. Vitelli, F. Asaro, L. Feruglio, *J. Phys. Chem. B* **2004**, *108*, 8960.
[34] a) A. Mohraz, *Curr. Opin. Colloid Interface Sci.* **2016**, *25*, 89; b) A. Toor, S. Lamb, B. A. Helms, T. P. Russell, *ACS Nano* **2018**, *12*, 2365.
[35] A. S. Basu, *Lab Chip* **2013**, *13*, 1892.
[36] a) G. M. Meconi, N. Ballard, J. M. Asua, R. Zangi, *Soft Matter* **2016**, *12*, 9692; b) S. F. Turner, S. M. Clarke, A. R. Rennie, P. N. Thirtle, D. J. Cooke, Z. X. Li, R. K. Thomas, *Langmuir* **1999**, *15*, 1017.
[37] H. Wu, J. Xie, M. Morbidelli, *Soft Matter* **2013**, *9*, 4437.
[38] A. Cingolani, D. Cuccato, G. Storti, M. Morbidelli, *Macromol. Mater. Eng.* **2018**, *303*, 1700417.
[39] O. J. Dressler, P. D. Howes, J. Choo, A. J. deMello, *ACS Omega* **2018**, *3*, 10084.

